Validity of SLAC fermions for the (1 + 1)-dimensional helical Luttinger liquid

Zhenjiu Wang,[1,*] Fakher Assaad,[2,3,†] and Maksim Ulybyshev[2,‡]
[1]*Max-Planck-Institut für Physik komplexer Systeme, Dresden 01187, Germany*
[2]*Institut für Theoretische Physik und Astrophysik, Universität Würzburg, 97074 Würzburg, Germany*
[3]*Würzburg-Dresden Cluster of Excellence ct.qmat, Am Hubland, 97074 Würzburg, Germany*

(Received 24 November 2022; revised 5 May 2023; accepted 21 June 2023; published 5 July 2023)

The Nielson-Ninomiya theorem states that a chirally invariant free fermion lattice action, which is local, translation invariant, and real, necessarily has fermion doubling. The SLAC approach gives up on locality, and long-range hopping leads to a linear dispersion with singularity at the zone boundary. We introduce a SLAC Hamiltonian formulation that is expected to realize a U(1) helical Luttinger liquid in a naive continuum limit. We argue that nonlocality and concomitant singularity at the zone edge have important implications. Large momentum transfers yield spurious features already in the noninteracting case. Upon switching on interactions, nonlocality invalidates the Mermin-Wagner theorem and allows for long-ranged magnetic ordering. In fact, in the strong-coupling limit the model maps onto an XXZ-spin chain with $1/r^2$ exchange. Here, both spin-wave and DMRG calculations support long-ranged order. While the long-ranged order opens a single-particle gap at the Dirac point, the singularity at the zone boundary persists for any finite value of the interaction strength such that the ground state remains metallic. Hence, the SLAC Hamiltonian does not flow to the 1D helical Luttinger liquid fixed point. Aside from DMRG simulations, we have used auxiliary field quantum Monte Carlo simulations to arrive at the above conclusions.

DOI: 10.1103/PhysRevB.108.045105

I. INTRODUCTION

The Nielson-Ninomiya theorem states that a chirally invariant free fermion lattice action, which is local, translation invariant, and real, necessarily has fermion doubling [1]. How should one then carry out simulations of a single Dirac cone? A possible route is to consider higher dimensions. A single Dirac cone in say $1+1$ dimensions can be realized as a surface state of a $(2+1)$-dimensional topological insulator. The other Dirac cone lies on the other surface and as the system size grows, mixing between the cones will vanish such that the physics of a single cone can be studied. In the realm of high-energy physics, this construction is referred to as domain wall fermions [2]. In the domain of the solid state, this idea has been used to study correlation effects in helical Luttinger liquids [3,4].

Alternatively one can violate the assumption of the locality of the fermion lattice action. This idea was put forward in the so-called SLAC lattice fermions, introduced in the 1970s and bearing the name derived from Stanford Linear Accelerator Center [5]. In this formulation, the locality of the lattice action is broken by the long-range hoppings, which decay as a power law of the distance between lattice sites. One can arrange this decay in a way that the Fermi velocity at one of the Dirac cones diverges and this "doubler" eventually shrinks into a singularity at the Brillouin zone boundary. This singularity is inevitable since, on a Bravais lattice, the dispersion relation is a periodic function of the reciprocal lattice vector. The question we will address in this article is whether the singularity at the zone boundary is a relevant perturbation. So-called SLAC fermions have been used in a number of solid-state [6–9] and high-energy physics [10–12] setups, and seem to provide a simple route to simulate a single Dirac cone in a lattice model with finite lattice constant a. In particular, this avoids the potentially expensive step of dealing with higher-dimensional systems. SLAC fermions come with a singularity at the Brillouin zone boundary at $k = \pm\pi/a$ in one dimension. The question we will ask in this article is how the nonlocality and concomitant singularity at the zone edge effects the physical results, in comparison to a domain wall fermion approach.

To do so, we will consider the simplest possible model, the helical Luttinger liquid emerging at the boundary of a 2D quantum spin Hall insulator as realized by the Kane-Mele model [13]. In particular we will consider a setup with U(1) symmetry, corresponding to conservation of z-total spin. This choice is challenging for SLAC fermions. For short-ranged interactions the Mermin-Wagner theorem states that continuous symmetries cannot be spontaneously broken in $1+1$ dimensions even in the zero-temperature limit. In fact, in conjunction with the intrinsic nesting instabilities of $(1+1)$-dimensional systems this impossibility of ordering leads to the

*zhwang@pks.mpg.de
†Fakher.Assaad@physik.uni-wuerzburg.de
‡Maksim.Ulybyshev@physik.uni-wuerzburg.de

fluctuation-dominated physics of the Luttinger liquid [14,15]. The nonlocality of SLAC fermions violates the assumptions of the Mermin-Wagner theorem and can hence lead to artifacts especially in the strong-coupling limit. We note that this has recently been pointed out in Ref. [9].

Another reason for the choice of this model is that its naive continuum limit, corresponding to ignoring the zone boundary singularity, can be solved exactly since only forward scattering is allowed. The results of the bosonization approach have been favorably compared to calculations based on domain wall fermions [3,4]. In this article we formulate a SLAC Hamiltonian that allows for negative-sign-free auxiliary field quantum Monte Carlo (QMC) simulations. The key question that we want to ask is, is it meaningful to compare between the physics of the SLAC Hamiltonian and the Luttinger liquid one?

The article is organized as follows. In Sec. II, we will discuss the SLAC formulation of the helical Luttinger liquid. Before discussing our results for the noninteracting and interacting cases in Sec. V, we will summarize the bosonization results in Sec. III and the technicalities of the Monte Carlo simulations in Sec. IV. In Sec. VI we discuss a simple model to understand our strong-coupling results. In Sec. VII we summarize the implications of our results. The article contains several appendices that demonstrate the absence of the negative-sign problem (Appendix A), discuss the scaling dimension of $\hat{S}_i^z$ as a function of the coupling strength (Appendix B), and provide a spin wave analysis of the long-ranged XXZ model (Appendix C).

II. SLAC FORMULATION OF THE HELICAL LIQUID

We consider the following one-dimensional model of length L and lattice constant a:

$$\hat{H} = -v_F \sum_{i=1}^{L} \sum_{r=-L/2}^{L/2} t(r)(\hat{a}_i^\dagger \hat{b}_{i+r} + \hat{b}_{i+r}^\dagger \hat{a}_i) + U \sum_i \left(\hat{n}_i^a - \frac{1}{2}\right)\left(\hat{n}_i^b - \frac{1}{2}\right) \tag{1}$$

with

$$t(r) = (-1)^r \frac{\pi}{L \sin(r\pi/L)} \quad \text{for } r \neq 0 \text{ and } t(0) = 0. \tag{2}$$

Each unit cell harbors two orbitals, and $\hat{a}_i^\dagger$, $\hat{b}_i^\dagger$ are spinless fermion creation operators.

Using periodic boundary conditions and Fourier transformation

$$\begin{pmatrix} \hat{a}_k \\ \hat{b}_k \end{pmatrix} = \frac{1}{\sqrt{N}} \sum_{j=1}^{L} e^{ikj} \begin{pmatrix} \hat{a}_j \\ \hat{b}_j \end{pmatrix} \tag{3}$$

gives, up to a constant,

$$\hat{H} = -v_F \sum_{k=-\frac{\pi}{a}}^{\frac{\pi}{a}} t(k)(\hat{a}_k^\dagger, \hat{b}_k^\dagger)\sigma^y \begin{pmatrix} \hat{a}_k \\ \hat{b}_k \end{pmatrix} - \frac{U}{2} \sum_i \left[(\hat{a}_i^\dagger, \hat{b}_i^\dagger)\sigma^x \begin{pmatrix} \hat{a}_i \\ \hat{b}_i \end{pmatrix} \right]^2 \tag{4}$$

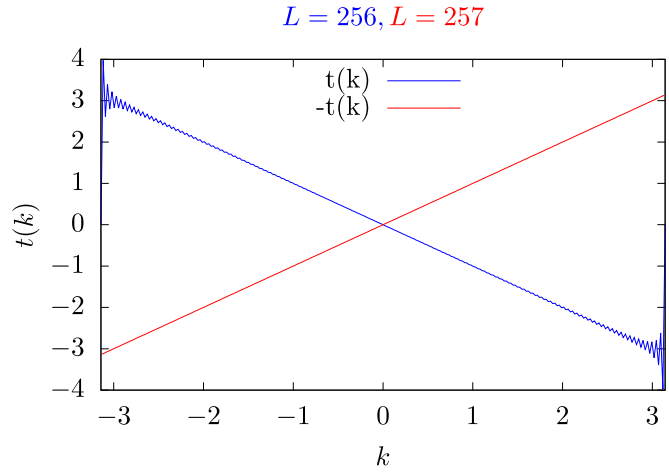

FIG. 1. $t(k)$ for even and odd lattices. The Gibbs phenomenon is apparent on even lattices. Here we set $a = 1$.

with

$$t(k) = i \sum_{r=-L/2}^{L/2} e^{-ikr} t(r). \tag{5}$$

In the above, $L = Na$. For any lattice size, $t(k)$ is a real and odd function. It is plotted in Fig. 1 and as apparent scales to $t(k) = k$ for k in the f Brillouin zone (BZ) and in the thermodynamic limit. One will also notice the Gibbs phenomenon (on even lattices) at the zone boundary associated to the discontinuity of $t(k)$. The rotation

$$\begin{pmatrix} \hat{a}_i \\ \hat{b}_i \end{pmatrix} = \frac{1}{\sqrt{2}}(1 + \sigma^x) \begin{pmatrix} \hat{c}_{i,\uparrow} \\ \hat{c}_{i,\downarrow} \end{pmatrix} \tag{6}$$

gives

$$\hat{H} = -v_F \sum_{k \in BZ, \sigma} \sigma k \hat{c}_{k,\sigma}^\dagger \hat{c}_{k,\sigma} + U \sum_i (\hat{n}_{i,\uparrow} - 1/2)(\hat{n}_{i,\downarrow} - 1/2), \tag{7}$$

corresponding to a helical liquid with Hubbard interaction. Our goal is to investigate whether the SLAC approach indeed reproduces the expected results obtained from bosonization of the helical liquid.

III. RESULTS FROM BOSONIZATION

Let us start by stating the bosonization [4,15] results valid in the continuum limit, $a \to 0$. In this limit, the fermion field operator reads

$$\hat{\Psi}_\sigma(x) = e^{ik_f x} \hat{R}(x) \delta_{\sigma,\uparrow} + e^{-ik_f x} \hat{L}(x) \delta_{\sigma,\downarrow}, \tag{8}$$

where $\hat{R}(x)$ and $\hat{L}(x)$ are independent right- and left-propagating fermion operators with spin and direction of motion locked in. Inserting the above form in Eq. (7) gives

$$\hat{H} = -v_F \sum_k k(\hat{R}_k^\dagger \hat{R}_k - \hat{L}_k^\dagger \hat{L}_k) + Ua \int_0^L dx\, \hat{R}^\dagger(x)\hat{R}(x)\hat{L}^\dagger(x)\hat{L}(x), \tag{9}$$

where $\hat{R}_k = \frac{1}{L}\int_0^L dx\, e^{ikx}\hat{R}(x)$. For a short-ranged model with nearest-neighbor hopping matrix element t, $v_F = 2ta$. Hence, to obtain a well-defined continuum limit, we scale both t and U as $1/a$. Since we have taken the continuum limit, the sum over momenta is unbounded. The above forward-scattering model can be solved with bosonization techniques reviewed in Ref. [15]. Correlation functions are given by

$$\begin{aligned} C_n(r) &\equiv \langle \hat{n}(r)\hat{n}(0)\rangle \propto \frac{1}{r^2}, \\ C_{S^z}(r) &\equiv \langle \hat{S}^z(r)\hat{S}^z(0)\rangle \propto \frac{1}{r^2}, \\ C_{S^x}(r) &\equiv \langle \hat{S}^x(r)\hat{S}^x(0)\rangle \propto \frac{\cos(2k_f r)}{r^{2K_\rho}}, \\ C_\Delta(r) &\equiv \langle \mathrm{Re}\hat{\Delta}_r^\dagger \mathrm{Re}\hat{\Delta}_0\rangle \propto \frac{1}{r^{2/K_\rho}}. \end{aligned} \tag{10}$$

In the above K_ρ is an interaction-strength-dependent Luttinger liquid exponent, $\hat{n}(r) = \sum_\sigma \hat{c}^\dagger_{r,\sigma}\hat{c}_{r,\sigma}$, $\boldsymbol{S}(r) = \frac{1}{2}\boldsymbol{c}_r^\dagger \boldsymbol{\sigma} \boldsymbol{c}_r$ with $\boldsymbol{\sigma}$ a vector of Pauli spin matrices, and $\hat{\Delta}_r^\dagger = \hat{c}^\dagger_{r,\uparrow}\hat{c}^\dagger_{r,\downarrow}$. Here, $2k_f$ denotes the momentum difference of the left spin-up and right spin-down movers. This wave vector is naturally picked up in $C_{S^x}(r)$ since it involves scattering between the two branches. In our construction, $k_f = 0$. Before proceeding and as mentioned earlier the bosonization results are consistent with the domain wall fermion approach of [3,4] even in the rather strong coupling limit. The above will be our reference result and we will ask the question under which conditions we can reproduce it with the SLAC lattice regularization.

IV. QUANTUM MONTE CARLO SIMULATIONS

The Hamiltonian of Eq. (1) does not suffer from a negative-sign problem in QMC simulations [16,17]. To see this, one will rewrite the model as

$$\begin{aligned} \hat{H} = &- v_F \sum_{i=1}^{L}\sum_{r=-L/2}^{L/2} t(r)(\hat{a}_i^\dagger \hat{b}_{i+r} + \hat{b}_{i+r}^\dagger \hat{a}_i) \\ &- \frac{U}{2}\sum_i (\hat{a}_i^\dagger \hat{b}_i + \hat{b}_i^\dagger \hat{a}_i)^2, \end{aligned} \tag{11}$$

where we have omitted a constant. Next we adopt a Majorana representation,

$$\hat{a}_i = \frac{1}{2}(\hat{\gamma}_{i,1,1} + i\hat{\gamma}_{i,2,1}), \quad \hat{b}_i = -\frac{i}{2}(\hat{\gamma}_{i,1,2} + i\hat{\gamma}_{i,2,2}), \tag{12}$$

to obtain

$$\hat{H} = v_F \sum_{i=1}^{L}\sum_{r=-L/2}^{L/2} t(r)\frac{i}{4}\hat{\boldsymbol{\gamma}}_i^T \tau_x \hat{\boldsymbol{\gamma}}_{i+r} - \frac{U}{2}\sum_i \left(\frac{1}{4}\hat{\boldsymbol{\gamma}}_i^T \tau_y \hat{\boldsymbol{\gamma}}_i\right)^2, \tag{13}$$

where $\hat{\boldsymbol{\gamma}}_i^T = (\hat{\gamma}_{i,1,1}, \hat{\gamma}_{i,2,1}, \hat{\gamma}_{i,1,2}, \hat{\gamma}_{i,2,2})$. Here we have used the fact that $t(r)$ is an odd function of r and adopted the notation $\hat{\gamma}_{i,\sigma,\tau}$ where the Pauli τ (σ) matrices act of the τ (σ) indices. A global O(2) symmetry in the σ indices now becomes apparent. After a real Hubbard-Stratonovich transformation of the perfect square, the fermion determinant will be given by the square of a Pfaffian. Since one will show that the Pfaffian is real, we will conclude in the absence of the negative-sign problem. Hence the absence of the sign problem for this SLAC model of the helical liquid follows the same logic as for the so-called spinless t-V model [18,19]. In Appendix A we show the absence of the sign problem for the generic model:

$$\begin{aligned} \hat{H} = &- v_F \sum_{i=1}^{L}\sum_{r=-L/2}^{L/2} t(r)(\hat{a}_i^\dagger \hat{b}_{i+r} + \hat{b}_{i+r}^\dagger \hat{a}_i) \\ &- \frac{U}{2}\sum_i [(\hat{a}_i^\dagger, \hat{b}_i^\dagger)\sigma_\alpha(\hat{b}_i, \hat{a}_i)^T]^2, \end{aligned} \tag{14}$$

where σ_α is a Pauli spin matrix. Note that after computing the square one will explicitly see that the Hamiltonian is α independent. For any value of α, we can use the ALF [20] implementation of the finite-temperature auxiliary field QMC algorithm [21–24]. In fact, Eq. (14), which formulates the interaction in terms of a perfect square, has the required form for usage of the ALF library, and concomitant Hubbard-Stratonovich transformation.

As mentioned above, the results are α independent. However, the Monte Carlo Markov chain will have a strong α dependence. We have seen that we obtain the best results when considering the σ_y formulation. This stems from the fact that after the rotation of Eq. (6) the U(1) symmetry of the helical liquid is satisfied for each Hubbard-Stratonovich field configuration.

We also would like to stress that since we are working in the Hamiltonian formulation, the resulting Lagrangian has SLAC hoppings only in the spatial direction and is local along the Euclidean time direction.

We used the interaction strength (bandwidth) as the energy unit for simulations at large (small) values of U/v_F. For $U/v_F \leqslant 4$ we choose $v_F\beta = L$ and $v_F\Delta\tau = 0.1$, whereas for $U/v_F > 4$ we considered $U\beta/4 = L$ and $U\Delta\tau/4 = 0.1$.

V. RESULTS

We will show that the SLAC approach suffers from two basic issues.

The first one can be seen already in the noninteracting limit and originates from processes with large momentum transfer. This deficiency can be illustrated as the violation of the anomaly relation in the lattice Schwinger model with SLAC fermions [25]. If we consider the continuum theory and turn on a constant electrical field pointing to the right, the right movers will acquire momentum and energy and will fill their branch of the dispersion relation up to some positive level. At the same time the left movers will lose energy and hence their branch of the cone will be filled only up to the same but negative level. Thus the axial charge will appear as an imbalance between the right and left movers. However, this is not true for the SLAC fermions due to the finite size of the Brillouin zone and finite depth of the Dirac sea; e.g., the right movers at the bottom of the Dirac sea will also acquire energy and thus the very bottom of this branch of the dispersion relation will not be filled anymore. These effects will compensate the difference between right and left movers

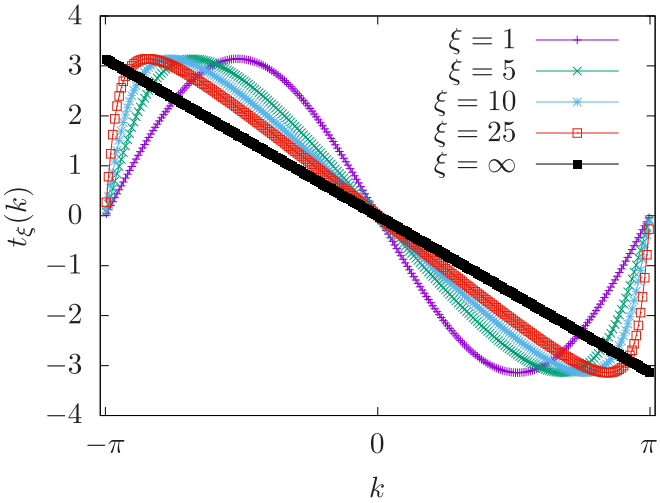

FIG. 2. k dependence of $t_\xi(k)$ for length scale $\xi = 1, 5, 10, 25$, and ∞. We took $L = 257$.

in the low-momentum modes leading to the axial charge being always zero. Though this is only a qualitative illustration, it shows the presence of the nontrivial dynamics near the edge of the Brillouin zone.

Another issue can be seen upon switching on intermediate to strong correlations as measured in unit of the bandwidth. In this case we observe a long-ranged order again contradicting the results from continuum theory.

Both points will be carefully studied in the subsequent subsections.

A. The noninteracting case

SLAC fermions become very transparent when introducing a length scale ξ in the hopping:

$$t_\xi(r) = t_0(\xi)\frac{(-1)^{r/a}\pi}{\frac{L}{a}\sin(r\pi/L)}e^{-\sin(r\pi/L)/\xi} \tag{15}$$

(see Fig. 2). In the above, we adjust $t_0(\xi)$ so as to fix the bandwidth to 2π. Clearly, the Fourier transform of a short-range function has to be smooth and one will see that for any finite value of ξ we observe two crossings of the Fermi surface albeit with very different values of the velocity. In fact the velocity at the zone boundary diverges with growing values of ξ. In principle, for any finite value of ξ we expect umklapp processes to be relevant such that any finite value of U should lead to an insulating state. However, since the velocity at the zone boundary diverges as ξ, the phase space available to these umklapp processes will vanish in the $\xi \to \infty$ limit. Another consequence of the singularity at the zone boundary is that *large* momentum transfer will always provide a discrepancy with the bosonization even in the noninteracting case. One can illustrate this by considering the charge-charge correlation functions for the SLAC Hamiltonian for the half-filled case, $\mu = 0$, at zero temperature:

$$\langle \hat{n}(r)\hat{n}(0)\rangle = \frac{1}{2\pi^2}\frac{\cos(\pi r) - 1}{r^2}. \tag{16}$$

In the above $\hat{n}(r) = \sum_\sigma \hat{c}^\dagger_{r,\sigma}\hat{c}_{r,\sigma}$. This result is independent of the value of ξ and merely relies on the fact that the dispersion relation intersects the Fermi energy at wave vectors $k = 0$ and $k = \frac{\pi}{a}$. The above expression already deviates from the bosonization result Eq. (10) and shows that already at this level one will obtain the same result as for the continuum model, where the zone edge diverges, only if one blocks large momentum transfers. This can be done by introducing point-splitting operators on the lattice, as was already suggested in [12,26].

B. Monte Carlo results

We have computed the structure factors

$$S_\bullet(k) = \sum_r e^{ikr}C_\bullet(r), \tag{17}$$

where the bullet refers to charge, spin along the z- or x-spin quantization axis, or paring correlations [see Eq. (10)]. To obtain an estimate of the power-law decay at a given wave vector, one can consider

$$B_\bullet(k, L/2) \equiv 2C_\bullet(k) - C_\bullet(k + 2\pi/L) - C_\bullet(k - 2\pi/L). \tag{18}$$

$\frac{L}{2\pi}B_\bullet(k, L/2)$ corresponds to the left minus the right derivative at a given k vector. Hence for a smooth function this quantity scales to zero as a function of system size. However for k vectors where one observes a cusp, it will scale to a finite value. One will show that

$$C_\bullet(L/2) = \frac{1}{4L}\sum_k e^{ikL/2}B_\bullet(k, L/2) \tag{19}$$

such that the scaling of $B_\bullet(k, L/2)$ at wave vectors k where one observes a cusp will reflect the decay of the correlation function [27] at this wave vector.

Figure 3 plots the real- and k-space correlation functions for the above-mentioned quantities. To better understand the results, we consider the behavior of the cusps in the corresponding structure factors by plotting $B_\bullet(k = 0, L/2)$ as a function of system size and coupling strength.

Let us start with the charge. From Fig. 3(a) we see that irrespective of the coupling constant in the range $U \in [0, 10]$ the real-space charge correlation decays as $1/r^2$. In the weak-coupling limit we observe a $(-1)^r$ modulation alongside the uniform decay. This weak-coupling behavior gives way to a uniform decay at strong coupling. In k space, Fig. 3(f), we see that the cusp at $k = \pi$ rounds off as a function of growing interaction strength but that the cusp at $q = 0$ remains robust. We also notice that as a function of growing interaction strength the charge response is suppressed. We can pin down the charge exponent by analyzing $LB_n(k = 0, L/2)$ in Fig. 4(a). Irrespective of the interaction strength, it is to an accurate degree L independent, thus reflecting a $1/r^2$ decay of the charge correlations.

At weak coupling the z component of spin is very similar to the charge (at $U = 0$ they are identical); see Figs. 3(c) and 3(h). In contrast however, the cusp at $k = 0$ becomes more pronounced at strong coupling. Figure 4(c) shows that the z-spin correlations acquire a nontrivial exponent in the

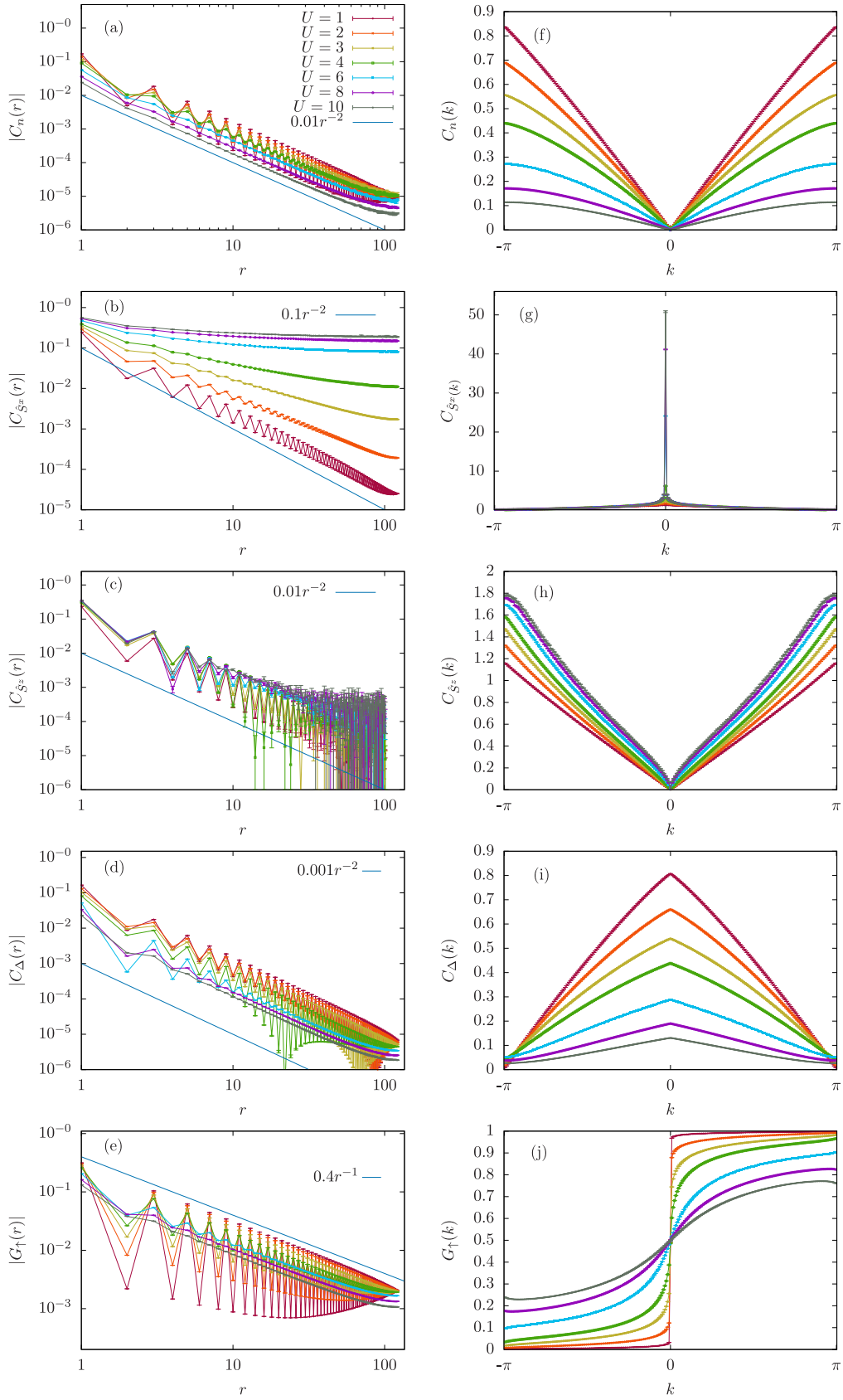

FIG. 3. Real-space correlation functions (a)–(e) and corresponding structure factors (f)–(j). Here we consider the charge, C_n, x (z) component of spin C_{S^x} (C_{S^z}), and pairing C_Δ and single-particle $G_\uparrow$ correlation functions. All the panels share the same legend color as the one in (a). For C_n, C_{S^x}, C_Δ, and $G_\uparrow$, we chose $L = 243$, whereas for C_{S^z}, we considered $L = 203$. The reason for this mismatch is large fluctuations in the QMC runs for C_{S^z} and for large sizes.

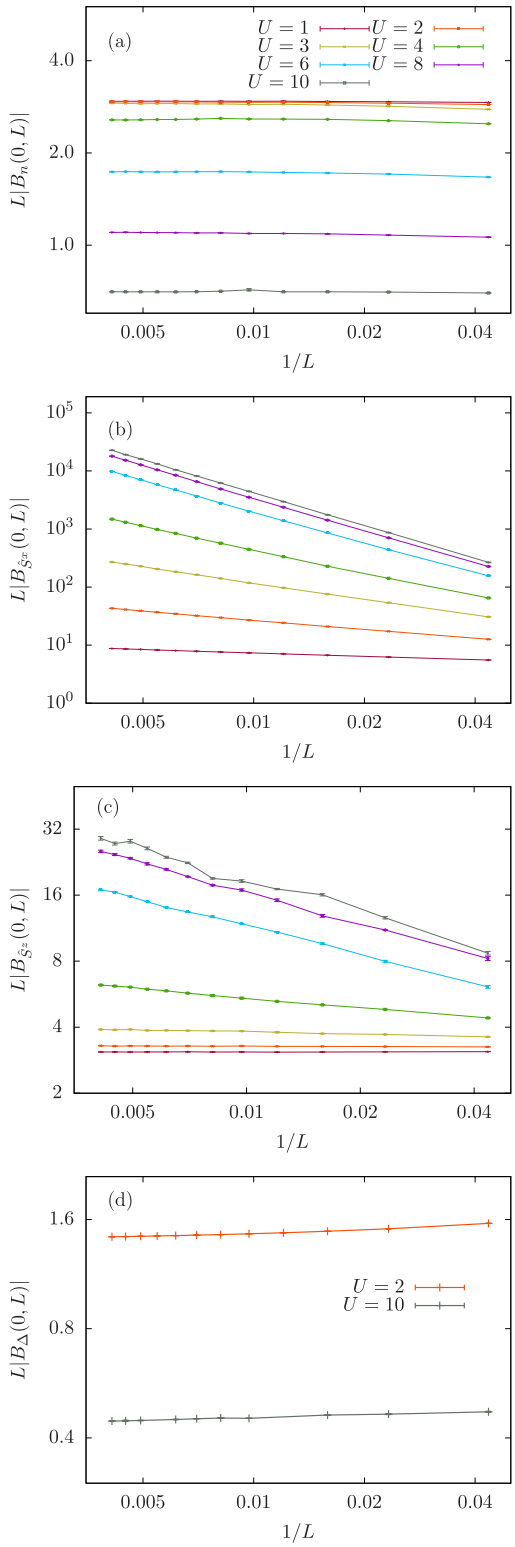

FIG. 4. $B(k = 0, L)L$ as function of $1/L$ for charge (a), $\hat{S}^x$ (b), $\hat{S}^z$ (c), and pairing (d). (b) and (c) share the same legend color as the one in (a).

strong-coupling limit. This stands at odds with the bosonization result of Eq. (10).

The spin correlations along the x-spin quantization, Figs. 3(b) and 3(g), direction are the most intriguing results. At weak coupling and on our system sizes, this correlation function follows roughly a $1/r^2$ form consistent with $LB_{S^x}(k = 0, L)$ constant, Fig. 4(b). $LB_{S^x}(k = 0, L/2)$ has a marked U dependence. It is remarkable to see that at strong coupling $LB_{S^x}(k = 0, L/2) \propto L^2$, thus suggesting long-range magnetic order as is confirmed by the very strong peak in the structure factor at $k = 0$ and the lack of decay in real space. We note that $LB_{S^x}(k = 0, L/2) \propto L^2$ is consistent with $C_{S^x}(k = 0) \propto L$. This result seems at odds with the Mermin-Wagner theorem, which states that a continuous symmetry cannot be broken at $T = 0$ in the ground state. However, the assumptions for the theorem to be valid require *short-ranged* interactions. The nonlocality of the SLAC fermions may very well invalidate this assumption. We note that long-range order can be stabilized by coupling spin chains locally to an ohmic bath, thus introducing long-ranged interactions along the imaginary time [28].

Long-ranged order along the x-spin quantization axis breaks time-reversal symmetry and allows for elastic scattering between the right-moving spin-down and left-moving spin-up electrons. At the single-particle, mean-field level, we expect

$$\hat{H}_{MF} = \sum_{k=-\frac{\pi}{a}}^{\frac{\pi}{a}} \hat{\boldsymbol{c}}_k^\dagger [-v_f k \sigma_z + m_x \sigma_x] \hat{\boldsymbol{c}}_k, \tag{20}$$

where m_x denotes the ordered moment. This symmetry breaking generates a mass gap at the Fermi momentum $k_f = 0$: $E_k = \pm\sqrt{(v_f k)^2 + (m_x)^2}$. Figure 3(j) plots the single-particle equal-time Green function, $G_\sigma(k) = \langle \hat{c}_{k,\sigma}^\dagger \hat{c}_{k,\sigma} \rangle$. As U grows, the singularity at $k = 0$ evolves to a smooth feature. Figure 3(e) confirms this: at weak coupling, $G_\sigma(r) \propto 1/r$ as expected for Dirac electrons in $(1 + 1)$D, and in the strong-coupling limit the L-independent form of $LB(k = 0, L)$ is consistent with a mass gap. $G_\sigma(k)$ has another singularity at $k = \pi$ that dominates the long-ranged real-space behavior. Putting all together, the data in the strong-coupling limit are consistent with the form $G_\sigma(r) \propto [ae^{-r/\xi} + (-1)^r]/r$, where ξ is set by the inverse ordered moment m_x. We also notice that the overall amplitude of $G_\sigma(r)$ diminishes as a function of U in the strong coupling.

Finally, we consider the pairing correlations in Figs. 3(d) and 3(i) as well as in Fig. 4(d). We again observe nonanalyticities at $k = 0$ and $k = \pi$ in the structure factor. The nonanalytical behavior at $k = 0$ survives the strong-coupling limit, whereas $C_\Delta(k)$ evolves toward a smooth function in the vicinity of $k = \pi$. The singularity at $k = 0$ leads to a $1/r^2$ decay of the pair correlation, and again the overall amplitude of the correlation function decreases as as function of increasing U.

VI. INTERPRETATION OF THE STRONG-COUPLING LIMIT

In this section, we provide a consistent interpretation of the strong-coupling limit. In this limit the QMC data show long-ranged magnetic ordering along the x-spin quantization axis. The single-particle Green function decays as $(-1)^r/r$, and the density as well as the pairing correlations follow a $1/r^2$

law. On the other hand the z component of spin correlations has a power-law decay with the exponent depending on the interaction strength. Clearly this behavior lies at odds with the bosonization results.

Our simulations show that the ground is a metal with long-ranged magnetic order. To best understand our results, let us start with a mean-field representation of this strong-coupling ground state:

$$|\Psi_0\rangle = \prod_r \frac{1}{\sqrt{2}}(\hat{c}^\dagger_{r,\uparrow} + \hat{c}^\dagger_{r,\downarrow})|0\rangle. \tag{21}$$

Since the above wave function has no charge fluctuations and precisely one electron per site it is the ground state of the Hubbard interaction term, $\hat{H}_U$, with energy E_0.[1] Consider the small-hopping limit such that the ground-state wave function can be estimated perturbatively in the hopping $\hat{H}_t$ [29]:

$$|\Psi\rangle = |\Psi_0\rangle + \hat{Q}_0 \frac{1}{\hat{H}_U - E_0}\hat{Q}_0\hat{H}_t|\Psi_0\rangle. \tag{22}$$

In the above $\hat{Q}_0 = 1 - |\Psi_0\rangle\langle\Psi_0|$. Let us now compute the charge fluctuations, $C_n(r) = \langle\Psi|(\hat{n}_r - 1)(\hat{n}_0 - 1)|\Psi\rangle$ for $r \neq 0$. The sole contribution reads

$$C_n(r) = \langle\Psi_0|\hat{H}_t\hat{Q}_0\frac{1}{\hat{H}_U - E_0}\hat{Q}_0(\hat{n}_r - 1)(\hat{n}_0 - 1) \times \hat{Q}_0\frac{1}{\hat{H}_U - E_0}\hat{Q}_0\hat{H}_t|\Psi_0\rangle. \tag{23}$$

Since $\hat{H}_t$ has hopping processes on all length scales it contains the operator $t(r)\sum_\sigma \sigma\hat{c}^\dagger_{r,\sigma}\hat{c}_{0,\sigma}$. Applied on $|\Psi_0\rangle$ it will generate a doublon-holon pair at distance r with an energy cost with respect to E_0 set by U. This charge fluctuation will be picked up by $(\hat{n}_r - 1)(\hat{n}_0 - 1)$. Finally the doublon-holon pair will be destroyed by the operator $t(r)\sum_\sigma \sigma\hat{c}^\dagger_{0,\sigma}\hat{c}_{r,\sigma}$ again contained in $\hat{H}_t$. As a result, we estimate

$$C_n(r) \simeq \frac{t^2(r)}{U^2} \propto \frac{1}{U^2 r^2}. \tag{24}$$

The power law is confirmed by the QMC data of Fig. 3(a). It is also interesting to note that the magnitude of the charge-charge correlations are predicted to scale as $1/U^2$. Comparison between the $U = 6$ and $U = 10$ data in Fig. 3(f) supports this scaling.

The very same argument can be carried out for the pairing correlations. Let us pick up the above argument at the point where doublon is created on site r and a holon on site 0. Applying the pairing operator $\hat{\Delta}_r\hat{\Delta}^\dagger_0$ on this state will yield a nonzero result and transfer the doublon (holon) to the origin (site r). The operator $t(r)\sum_\sigma \sigma\hat{c}^\dagger_{r,\sigma}\hat{c}_{0,\sigma}$ will then annihilate the doublon-holon pair, and we will obtain a finite overlap with the mean-field ground state. Hence we also expect

$$C_\Delta(r) \simeq \frac{t^2(r)}{U^2} \propto \frac{1}{U^2 r^2} \tag{25}$$

in the strong-coupling limit, which is consistent with our QMC data, but inconsistent with the bosonization results Eq. (10).

We now consider the single-particle Green function. Here, the relevant terms in $\langle\Psi|\hat{c}^\dagger_{r,\sigma}\hat{c}_{0,\sigma}|\Psi\rangle$ are the mixed terms of the form

$$\langle\Psi_0|\hat{c}^\dagger_{r,\sigma}\hat{c}_{0,\sigma}\hat{Q}_0\frac{1}{\hat{H}_U - E_0}\hat{Q}_0\hat{H}_t|\Psi_0\rangle. \tag{26}$$

The doublon-holon pair created by $\hat{H}_t$ will be annihilated by the single-particle transfer $\hat{c}^\dagger_{r,\sigma}\hat{c}_{0,\sigma}$. In accordance with the QMC results this approximation gives

$$G_\sigma(r) \propto \frac{t(r)}{U} \propto \frac{(-1)^r}{Ur}. \tag{27}$$

We now comment on the nature, metallic or insulating, of the strong-coupling wave function. The very fact that the charge correlations follow a power law suggests a metallic ground state. An accepted definition of an insulating or metallic state is the Drude weight [30], which probes the localization of the wave function. Here, one considers a ring geometry and threads a magnetic flux Φ through the center of the ring. Such a flux will have an effect if the charge carriers are delocalized and can circle around it and, owing to the Aharonov-Bohm effect, acquire a phase factor $e^{2\pi i\Phi/\Phi_0}$ where Φ_0 is the flux quanta. Here we assume that the charge carriers have the electron charge. The Drude weight in d spatial dimensions is defined as

$$D(L) = \frac{1}{L^{d-2}}\frac{\partial^2 E_0(\Phi)}{\partial\Phi^2}\bigg|_{\Phi=0}. \tag{28}$$

For the insulating state $D(L)$ vanishes exponentially with L reflecting the localization length of the wave function. For a metallic state the Drude weight is finite. Let us now use this accepted criterion to the SLAC fermions, in the strong-coupling limit. A glimpse at the wave function in second-order perturbation theory [see Eq. (22)] shows that it contains holon-doublon excitations, at all length scales. The fact that they are costly in energy means that they are short lived, but during this short time, they can propagate over large distances due to the nonlocality of the hopping. Hence we expect the Drude weight to be finite. To substantiate this statement we carry out the following estimations. The flux leads to a twist in the boundary condition,

$$\hat{c}_{r+L,\sigma} = e^{2\pi i\frac{\Phi}{\Phi_0}}\hat{c}_{r,\sigma}, \tag{29}$$

which we can get rid of with the canonical transformation

$$\hat{d}_{r,\sigma} = e^{-2\pi i\frac{\Phi}{\Phi_0}\frac{r}{L}}\hat{c}_{r,\sigma}. \tag{30}$$

Under this canonical transformation, the Hubbard term remains invariant, the hopping reads

$$\hat{H}_t(\Phi) = v_F i\sum_{i,\sigma}\sum_r \sigma t(r)\hat{d}^\dagger_{i,\sigma}\hat{d}_{i+r,\sigma}e^{2\pi i\frac{\Phi}{\Phi_0}\frac{r}{L}}, \tag{31}$$

and $\hat{d}_{r,\sigma}$ satisfies periodic boundary conditions: $\hat{d}_{r,\sigma} = \hat{d}_{r+L,\sigma}$. Let us now compute the second-order contribution to the energy that will pick up the dependence on the flux:

$$E_2(\Phi) = \langle\Psi_0|\hat{H}_t(\Phi)\hat{Q}_0\frac{1}{\hat{H}_U - E_0}\hat{Q}_0\hat{H}_t(\Phi)|\Psi_0\rangle. \tag{32}$$

[1]Here we omit spin fluctuations discussed at length in Appendices B and C.

Starting from $|\Psi_0\rangle$ one will create for example a holon at position i and a doublon at position $i+r$ by applying the hopping. This process has matrix element $iv_F t(r) e^{-2\pi i \frac{\Phi}{\Phi_0}\frac{r}{L}}$ and energy cost set by U. The only way to perceive the flux is for the charge excitation to encircle it. Hence the second hopping process should destroy the doublon in favor of single occupancy at site $i+r$ and create an electron at site $i+L \equiv i$ thereby restoring single occupancy on this site such that the overlap with $|\Psi_0\rangle$ does not vanish. This second process comes with the matrix element $iv_F t(L-r) e^{-2\pi i \frac{\Phi}{\Phi_0}\frac{L-r}{L}}$. Putting everything together one obtains

$$E_2(\Phi) \propto -\frac{v_F^2}{U} \sum_i \sum_r t(r) t(L-r) \cos\left(2\pi \frac{\Phi}{\Phi_0}\right). \quad (33)$$

We hence see that in this approximation, the Drude weight reads

$$D \propto L^2 \left(\frac{2\pi}{\Phi_0}\right)^2 \frac{v_F^2}{U} \sum_r t(r) t(L-r). \quad (34)$$

One will check that $\sum_r t(r)t(L-r)$ takes a finite value. Hence we obtain the result that the Drude weight actually diverges as L^2, and only at $U=\infty$ will we have an insulating state on any finite lattice.

The above real-space picture does not provide an explanation of the observed power-law decay of the spin correlations along the z-quantization axis. Our perturbative calculation creates a doublon-holon pair, and since these excitations carry no spin, $C_{S^z}(r)$ vanishes identically. To go beyond this approximation, we can consider the Hamiltonian of Eq. (20). In fact in the limit $U \to \infty$ this approximation will reproduce the above perturbative results. Given Eq. (20) we can compute $C_{S^z}(r)$ to obtain

$$C_{S^z}(r) = -\frac{1}{2}\left|\frac{1}{L}\sum_{p=-\frac{\pi}{a}}^{\frac{\pi}{a}} e^{-ipr} \frac{v_F p}{\sqrt{(v_F p)^2 + (U m_x)^2}}\right|^2. \quad (35)$$

The sum under the square corresponds to the single-particle Green function, which, due to the singularity at the Brillouin zone edge, decays as $1/r$ with a $(-1)^r$ modulation. Since the spin correlation is a particle-hole excitation, it decays as $1/r^2$ but with no spatial modulation. Furthermore, in the strong-coupling limit, the amplitude of the spin-spin correlations along the z-quantization axis would scale as $1/U^2$. The above stands at odds with the QMC data. As shown in Fig. 4, $C_{\hat{S}^z}$ seems to pick up a nontrivial scaling dimension in the sense that it decays slower than $1/r^2$, as U increases to a scale comparable to the bandwidth. Furthermore in the strong-coupling limit Fig. 3(h) shows that the amplitude of $C_{S^z}(k)$ grows as a function of increasing U. Hence, the data beg for another interpretation.

As seen above, in the limit $U \to \infty$ charge fluctuations are suppressed by a factor $1/U^2$ such that we can carry out a Schrieffer-Wolff transformation to obtain the Heisenberg model:

$$\hat{H}_{U\to\infty} = \frac{4v_f^2}{U} \sum_{i,r=-L/2}^{L/2} t^2(r)\left[\hat{S}_i^z \hat{S}_{i+r}^z - \hat{S}_i^x \hat{S}_{i+r}^x - \hat{S}_i^y \hat{S}_{i+r}^y\right]. \quad (36)$$

Since $t^2(r) \propto 1/r^2$ the conditions for the validity of the Mermin-Wagner theorem [31] are not satisfied. Furthermore, the spin interaction along the z direction is antiferromagnetic, thus leading to frustration due to the long-ranged nature of the exchange. Since in the transverse direction the coupling is ferromagnetic, frustration can be avoided by ordering in the x-y plane. In fact, spontaneous U(1) symmetry breaking of this spin model has been confirmed by numerical and renormalization group analysis [32], and naturally the magnetic ordering is reproduced by our simulations at the large-U limit.

Furthermore, in Appendix B, we systemically show extrapolation of $\hat{\Delta}_{S^z}$ as function of U: $\Delta_{\hat{S}^z}$ starts to deviate from 1 at intermediate ranges of U and approaches around 0.7 at the large-U limit. Hence fluctuations around the mean-field approach have to be taken into consideration. At this point, we only have solid understanding for the scaling behavior of the XXZ chain in the large-U limit. In Appendices B and C we carry out density matrix renormalization group simulations and linear spin-wave calculations, to show the scaling dimensions of $\hat{S}_i^z$, $\Delta_{\hat{S}^z} = 3/4$. As a consequence, the spin structure factor $C_{S^z}(k) \propto \sqrt{k}$ in the long-wavelength limit. This is consistent with the decay of scaling dimension in the SLAC system as strength of the interaction grows.

VII. DISCUSSION AND CONCLUSIONS

We introduce a one-dimensional toy model Hamiltonian based on the SLAC fermion approach. Our SLAC model differs from the $(1+1)$-dimensional helical liquid by a singularity at the Brillouin zone boundary. Although we originally aimed at benchmarking the validity of this approach in describing the $(1+1)$-dimensional helical liquid, a completely different fixed point is found. For this very specific case, we understand that the differences are present both in the weak- and strong-coupling limits. Hence the singularity at the zone boundary is a relevant perturbation at the $(1+1)$-dimensional helical liquid fixed point.

One-dimensional systems are generically nested. For the helical Luttinger liquid at $U=0$ of Eq. (7), this leads to $\chi_\perp(k=0,\omega=0) \propto \ln \frac{v_f}{k_B T}$. As a consequence, a mean-field approach to correlation effects will generate long-ranged magnetic order along the spin-x quantization axis and a charge gap. Both the charge gap and the ordered moment will follow an essential singularity in the weak-coupling limit.

For generic local one-dimensional models we know that the above Stoner arguments cannot be made due to the Mermin-Wagner theorem [31] that tells us that quantum fluctuations will destroy the ordering even in the ground state. For our specific case, continuous U(1) spin-symmetry breaking is not allowed. This competition between the Stoner instability and the Mermin-Wagner theorem is at the very origin of Luttinger liquid behavior generic to $(1+1)$D interacting systems. This is exemplified by the helical Luttinger liquid: a metallic state with no single-particle gap and an interaction-strength-dependent power-law decay of the spin-spin correlations in the transverse direction. We note that due to U(1) spin symmetry, umklapp processes are symmetry forbidden such that the system will remain metallic for arbitrary large interactions. This understanding of the helical Luttinger liquid has been confirmed numerically within a domain wall fermion

approach [3,4] in which interaction effects are included only on one set of domain wall fermions.

The nonlocality of the SLAC fermion approach brings major differences to the above picture. The key point is that it violates the assumptions of the Mermin-Wagner theorem. The violation of the Mermin-Wagner theorem in the realm of SLAC fermions was recently pointed out in Ref. [9]. Our numerical results explicitly confirm this in the strong-coupling limit where long-ranged magnetic order along the x-spin quantization axis and global U(1) spin symmetry breaking are observed. This allows for a mass term and in fact we observe a single-particle gap opening at the Fermi wave vector.

We should note that one can try to use the SLAC fermions in the context in which the continuous chiral symmetry is reduced to a Z_2 discrete one. For instance, such situation emerges when one considers more than one flavor of fermions in $(1+1)$D. If the interaction term is written as $(\bar{\psi}_a\psi_a)^2$, where ψ is a two-component spinor, the continuous symmetry is broken and only Z_2 symmetry remains. Analogously, the spin-orbit coupling will reduce the U(1) continuous symmetry to a Z_2 discrete one. In this case, the aforementioned issues of SLAC action with the Mermin-Wagner theorem will be waived. However, some artifacts will likely survive even for the discrete Z_2 symmetry. In particular, the deviation of the behavior of the correlation functions in Eq. (25) from the strong-coupling limit does not involve a continuous symmetry for its derivation. Hence these discrepancies will remain even for models with discrete symmetries. Another important point is the nature of the ordered state observed in our QMC simulations. In contrast to Dirac systems where magnetic mass terms are generated spontaneously [33], this ordered state remains metallic. This is again a consequence of nonlocality inherent to the SLAC approach that produces doublon-holon pairs at any length scale. Equivalently, the current operator becomes long-ranged. Strictly speaking Gross-Neveu transitions that have been studied in the realm of SLAC fermions [6,8,9] are not metal-to-insulator transitions but metal-to-metal ones.

At vanishing coupling strength, the results of the helical Luttinger liquid with $K_\rho = 1$ become exact provided that we block large momentum transfers. As mentioned above, this noninteracting point is unstable. An important question is to assess whether there is a finite value of U_c below which we will observe the physics of the helical Luttinger liquid. We conjecture that $U_c = 0$. As mentioned above, the noninteracting limit is unstable to ordering in the transverse spin direction. Since the nonlocality of the model leads to a violation of the Mermin-Wagner theorem quantum fluctuations will not destabilize the ordering and will not invalidate a Ginzburg-Landau mean-field picture. In this case, the local moment will be exponentially small in U/v_f such that exponentially large lattices will be required to detect it.

ACKNOWLEDGMENTS

We would like to thank L. Janssen, Z. Y. Meng, and A. Wipf for comments. Computational resources were provided by the Gauss Centre for Supercomputing e.V. [34] through the John von Neumann Institute for Computing (NIC) on the GCS Supercomputer JUWELS [35] at Jülich Supercomputing Centre (JSC). M.U. thanks the Deutsche Forschungsgemeinschaft (DFG) for financial support under Project No. UL444/2-1. F.F.A. acknowledges financial support from the DFG through the Würzburg-Dresden Cluster of Excellence on Complexity and Topology in Quantum Matter–*ct.qmat* (EXC 2147, Project No. 390858490) as well as the SFB 1170 on Topological and Correlated Electronics at Surfaces and Interfaces (Project No. 258499086).

APPENDIX A: ABSENCE OF NEGATIVE-SIGN PROBLEM

There are various ways of formulating the QMC. Although in principle equivalent, the various formulations will lead to different Markov time series. Thereby the autocorrelation time for a given observable may be formulation dependent. The various formulations stem from different ways of writing the interaction term:

$$\hat{H}_U = -\frac{U}{2}\sum_i [(\hat{a}_i^\dagger, \hat{b}_i^\dagger)\sigma_\alpha(\hat{b}_i, \hat{a}_i)^T]^2. \tag{A1}$$

In the above, $\hat{H}_U$ is independent of the choice of the Pauli spin matrix σ_α. For the repulsive values of $U > 0$, we can carry out a Hubbard-Stratonovich decomposition of the perfect square term to obtain

$$Z \propto \int D\{\phi(i,\tau)\} e^{-S_\alpha(\phi(i,\tau))} \tag{A2}$$

with

$$S_\alpha(\phi(i,\tau)) = \int_0^\beta d\tau \sum_i \frac{\phi^2(i,\tau)}{2U} - \ln \mathrm{Tr}\mathcal{T} e^{-\int_0^\beta d\tau \hat{h}_{,\alpha}(\tau)}, \tag{A3}$$

$$\hat{h}_\alpha(\tau) = \hat{H}_0 + \sum_i \phi(i,\tau)(\hat{a}_i^\dagger, \hat{b}_i^\dagger)\sigma_\alpha(\hat{b}_i, \hat{a}_i)^T, \tag{A4}$$

and

$$\hat{H}_0 = -v_F \sum_{i=1}^{L}\sum_{r=-L/2}^{L/2} t(r)(\hat{a}_i^\dagger \hat{b}_{i+r} + \hat{b}_{i+r}^\dagger \hat{a}_i). \tag{A5}$$

We again stress that the partition function is α independent but that $\hat{h}_\alpha(\tau)$ has an explicit α dependency.

Using the Majorana representation of Eq. (12) we obtain different expressions for various choices of α. Below we go through them one by one.

(i) σ_x. In this case,

$$\hat{h}_x(\tau) = v_F \sum_{i=1}^{L}\sum_{r=-L/2}^{L/2} \frac{it(r)}{4}\hat{\boldsymbol{\gamma}}_i^T \tau_x \hat{\boldsymbol{\gamma}}_{i+r} + \sum_i \frac{\phi(i,\tau)}{4}\hat{\boldsymbol{\gamma}}_i^T \tau_y \hat{\boldsymbol{\gamma}}_i. \tag{A6}$$

We see that the operators $\hat{T}^+$ and $\hat{T}^-$ with

$$\hat{T}^+ \gamma_i \hat{T}^{+,-1} = T^+ \gamma_i \quad \text{with } T^+ = i\tau_y\tau_x\sigma_x K \tag{A7}$$

and

$$\hat{T}^- \gamma_i \hat{T}^{-,-1} = T^- \gamma_i \quad \text{with } T^- = \tau_z i\sigma_y K, \tag{A8}$$

where K denotes complex conjugation, leave $\hat{h}(\tau)$ invariant. Furthermore $(T^\pm)^2 = \pm 1$ and $\{T^+, T^-\} = 0$. Hence according to Ref. [16] the Hamiltonian falls into the so-called Majorana class and does not suffer from the negative-sign problem.

(ii) σ_y. For this choice,

$$\hat{h}_y(\tau) = v_F \sum_{i=1}^{L} \sum_{r=-L/2}^{L/2} \frac{it(r)}{4} \hat{\boldsymbol{\gamma}}_i^T \tau_x \hat{\boldsymbol{\gamma}}_{i+r} + \sum_i \frac{\phi(i,\tau)}{4} \hat{\boldsymbol{\gamma}}_i^T \sigma_y \tau_x \hat{\boldsymbol{\gamma}}_i, \tag{A9}$$

such that we have to choose

$$T^- = i\tau_y K \quad \text{and} \quad T^+ = \tau_z K \tag{A10}$$

to show that the model is in the Majorana class.

(iii) σ_z. For this choice,

$$\hat{h}_z(\tau) = v_F \sum_{i=1}^{L} \sum_{r=-L/2}^{L/2} \frac{it(r)}{4} \hat{\boldsymbol{\gamma}}_i^T \tau_x \hat{\boldsymbol{\gamma}}_{i+r} - \sum_i \frac{\phi(i,\tau)}{4} \hat{\boldsymbol{\gamma}}_i^T \sigma_y \tau_z \hat{\boldsymbol{\gamma}}_i, \tag{A11}$$

such that we have to choose

$$T^- = i\tau_y K \quad \text{and} \quad T^+ = \tau_z \sigma_x K \tag{A12}$$

to show that the model is in the Majorana class.

APPENDIX B: SCALING DIMENSION OF $\hat{S}^z$ OPERATOR

Due to the systemic failure of the SLAC fermion approach in describing the physics of the $(1+1)$-dimensional helical Luttinger liquid, which is especially characterized by the spontaneous breaking of U(1) symmetry, we cannot expect the scaling behavior of the bosonization results of Eq. (10) to hold. Taking the $\hat{S}^z$ operator as an example, its equal-time structure factor shows a sharp (or smooth) cusp around $k = 0$ ($k = \pi$) as the interaction strength U increases, as depicted in Fig. 3(h). This indicates a violation of the $1/r^2$ scaling relation based on naive bosonization.

Generally the (equal-time) real-space correlation function of the $\hat{S}^z$ operator is

$$C_{\hat{S}^z}(r) = a r^{-2\Delta_0^{\hat{S}^z}} + b(-1)^r r^{-2\Delta_\pi^{\hat{S}^z}}, \tag{B1}$$

where $\Delta_0^{\hat{S}^z}$ and $\Delta_\pi^{\hat{S}^z}$ are the scaling dimensions at $k = 0$ and $k = \pi$, and a and b here are nonuniversal constants. We use the quantity $B_{\hat{S}^z}(k, L/2)$, as defined in Eq. (18), to extract the scaling dimension. In particular in the $L \to \infty$ limit we expect

$$B_{\hat{S}^z}(k = 0, L/2) \propto L^{-2\Delta_0^{\hat{S}^z}+1},$$
$$B_{\hat{S}^z}(k = \pi, L/2) \propto L^{-2\Delta_\pi^{\hat{S}^z}+1}. \tag{B2}$$

This approach for determining the scaling dimension relies on calculating the difference between the left and right derivatives of the structure factor. Therefore, it provides correct results within the range of $0.5 < \Delta \leqslant 1$. For $\Delta > 1$, the structure factor becomes a smooth function at the selected momentum point, making it difficult for our approach to distinguish between an exponential or power-law decay.

Figures 5(a) and 5(b) show that $B_{\hat{S}^z}(k = 0, L/2)$ scales linearly as a function of $1/L$, and its slope decreases in the large-U case, while $B_{\hat{S}^z}(k = \pi, L/2)$ behaves oppositely. The extrapolated scaling dimension, obtained by fitting the power-law function of Eq. (B2), is 1 within the error bars for $U < 3$. For $U > 3$, the values of $\Delta_{\hat{S}^z}$ systematically decrease (increase) for $k = 0$ ($k = \pi$), as shown in Fig. 5(c).

To verify the consistency of our results, we also conducted a density matrix renormalization group (DMRG) simulation

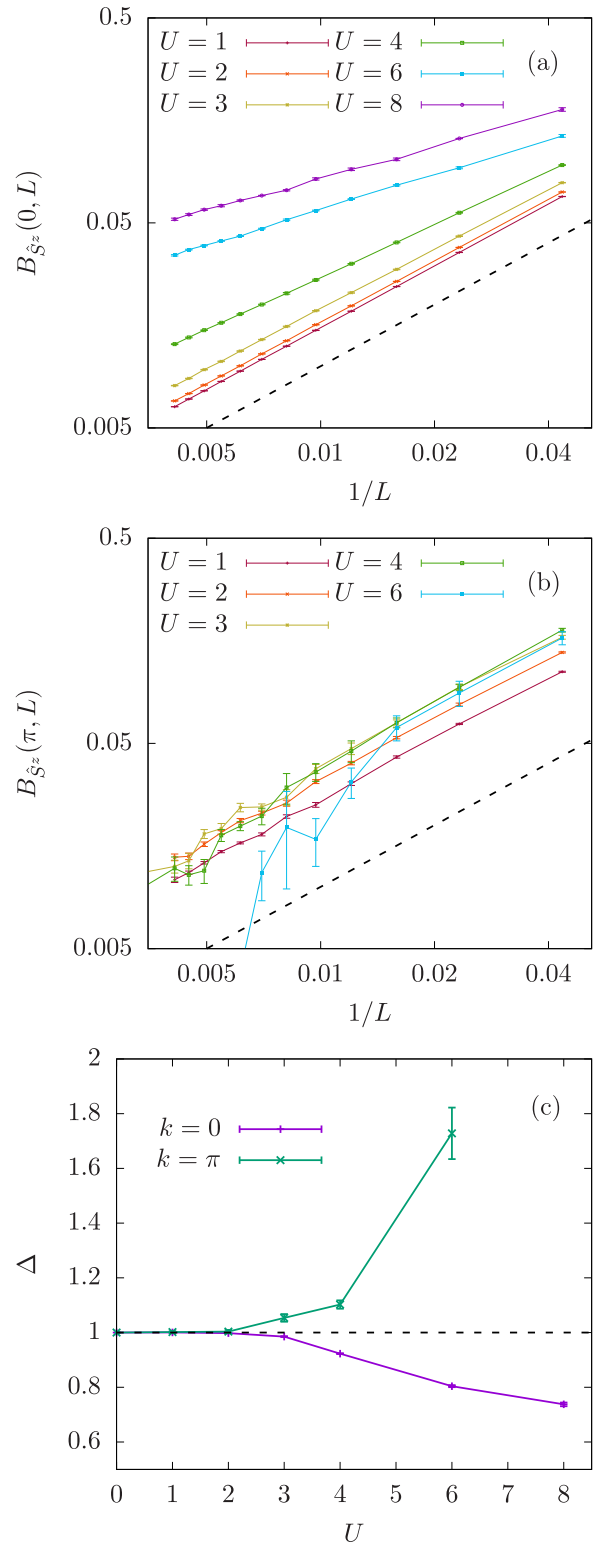

FIG. 5. $1/L$ dependence of $B_{\hat{S}^z}(k = 0, L/2)$ (a) and $B_{\hat{S}^z}(k = \pi, L/2)$ (b). The dashed line is $f(L) = 1/L$, as a guide to the eye. The extrapolated scaling dimension Δ_0 and Δ_π as a function of U is plotted in (c). The dashed line is $\Delta = 1$, as a guide to the eye.

of the one-dimensional XXZ chain with long-range interaction, which corresponds to the perturbed Hamiltonian of the SLAC system in the strong-coupling limit. Equation (36) in

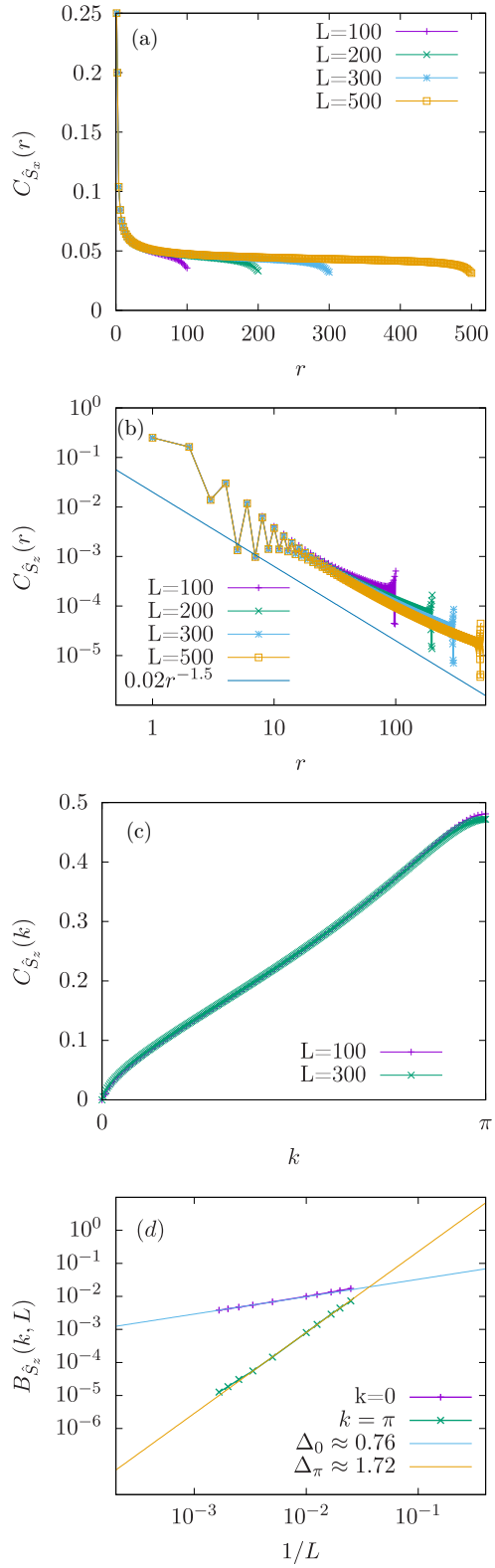

FIG. 6. Ground-state property of the XXZ chain based on DMRG simulation. (a) Real-space correlation function of $\hat{S}_x$ operator originated from the left boundary of the chain. (b) Same as (a), for $\hat{S}_z$ operator. The blue line plots function $0.02r^{-1.5}$ and is a guide to the eye. (c) Structure factor of the $\hat{S}_z$ operator. (d) $1/L$ dependence of $B_{\hat{S}_z}(k, L/2)$ for $k = 0$ and π in a logarithmic scale, as well as the two fitted function based on Eq. (B2) as guides to the eye.

the main text can be reformulated as

$$\hat{H}_{XXZ} = J \sum_{i,r\in\mathrm{OBC}} \frac{1}{r^2}\left[\hat{S}_i^z\hat{S}_{i+r}^z - \hat{S}_i^x\hat{S}_{i+r}^x - \hat{S}_i^y\hat{S}_{i+r}^y\right], \tag{B3}$$

where J is the only energy scale of the Hamiltonian and we set it to unity. Instead of the periodic boundary condition that is considered for the SLAC Hamiltonian, we consider an open boundary case here, such that the long-range interaction in Eq. (B3) is truncated at the boundary. We implemented the DMRG algorithm in the ITENSOR library [36]. The power-law nature of interaction in this system does not lead to a dramatic increase of entanglement in DMRG simulation, and we checked convergence for bond dimensions up to $\chi = 400$.

Figure 6(a) displays the long-range correlation of the $\hat{S}_x$ ($\hat{S}_y$) operator, which is consistent with our numerical results of the SLAC Hamiltonian in the large-U regime. On the other hand, the real-space decay of the $\hat{S}_z$ operator shows an algebraic scaling behavior, as shown in Figs. 6(b) and 6(c). It should be noted that the seemingly square root behavior of $C_{\hat{S}_z}(k)$ at $k \approx 0$ also fits well with the plot of the SLAC system in the large-U limit, as depicted in Fig. 3(h).

Finally, we also performed a scaling analysis for $B_{\hat{S}^z}(k, L/2)$ based on Eq. (B2). As shown in Fig. 6(d), $B_{\hat{S}^z}(k, L/2)$ displays a nice power-law behavior as a function of $1/L$. A collective fit based on Eq. (B2), using system sizes of $L = 200, 300, 400, 500, 600, 800$, and 1000, gives the scaling dimension of the $\hat{S}_z$ operator at $k = 0$:

$$\Delta_0^{\hat{S}^z} = 0.762(2). \tag{B4}$$

Note that at $k = \pi$ the $\Delta_\pi^{\hat{S}^z} > 1$ such that the structure factor at $k = \pi$ is a smooth function consistent with an exponential decay of staggered fluctuations.

APPENDIX C: SPIN-WAVE ANALYSIS OF THE $1/r^2$ XXZ CHAIN

In this Appendix, we carry out a spin-wave analysis of the XXZ model with $1/r^2$ exchange derived in Eq. (36). We will see that the long-ranged interaction stabilizes the order and that the scaling dimension of the $\hat{S}^z$ operator reproduces the DMRG results. We first carry out a canonical transformation,

$$\hat{\tilde{\boldsymbol{S}}}_i = R(\boldsymbol{e}_y, \pi/2)\hat{\boldsymbol{S}}_i, \tag{C1}$$

where $R(\boldsymbol{e}_y, \pi/2)$ is an SO(3) rotation around the axis $\boldsymbol{e}_y$ and with angle $\pi/2$ such that, e.g., $\hat{\tilde{S}}_i^z = \hat{S}_i^x$. Hence, Eq. (36) maps onto

$$\hat{H}_{XXZ} = \sum_{i,r=-L/2}^{L/2} J(r)\left[\hat{\tilde{S}}_i^x\hat{\tilde{S}}_{i+r}^x - \hat{\tilde{S}}_i^y\hat{\tilde{S}}_{i+r}^y - \hat{\tilde{S}}_i^z\hat{\tilde{S}}_{i+r}^z\right], \tag{C2}$$

with $J(r) = \frac{4v_f^2}{U}t^2(r)$. We will assume long-ranged ferromagnetic magnetic order along the $\hat{\tilde{S}}_i^z$ quantization axis and adopt the Holstein-Primakov representation:

$$\hat{\tilde{S}}_i^z = -\hat{b}_i^\dagger\hat{b}_i + S,$$
$$\hat{\tilde{S}}_i^+ = \sqrt{2S - \hat{b}_i^\dagger\hat{b}_i}\,\hat{b}_i, \tag{C3}$$

with $[\hat{b}_i, \hat{b}_j^\dagger] = \delta_{i,j}$. For small fluctuations around the ordered state, $\langle \hat{b}_i^\dagger \hat{b}_i \rangle \ll 2S$, we obtain

$$\hat{H}_{XXZ} = E_{MF} + S \sum_p \left(2J_0 \hat{b}_p^\dagger \hat{b}_p + J_p \hat{b}_{-p}^\dagger \hat{b}_p^\dagger + J_{-p} \hat{b}_{-p} \hat{b}_p \right) + \mathcal{O}(S^0). \tag{C4}$$

The first term corresponds to the Weiss mean-field energy, $E_{MF} = -\sum_{i,r} J(r) S^2$, and scales as S^2. The second term scales as S and describes spin-wave fluctuations with $J_p = \sum_r e^{ipr} J(r)$ and $\hat{b}_p = \frac{1}{\sqrt{L}} \sum_i e^{ipr} \hat{b}_i$. Lower orders in S are neglected. We diagonalize the above Hamiltonian with the Bogoliubov transformation,

$$\hat{a}_p^\dagger = \cosh(\theta_p) \hat{b}_p^\dagger + \sinh(\theta_p) \hat{b}_{-p} \tag{C5}$$

and

$$\tanh(2\theta_p) = \frac{J_p}{J_0}, \tag{C6}$$

to obtain

$$\hat{H}_{XXZ} = 2SJ_0 \sum_p \sqrt{1 - \frac{J_p^2}{J_0^2}}\, \hat{a}_p^\dagger \hat{a}_p + C \tag{C7}$$

up to a constant C. For the SLAC hopping of Eq. (2), $\frac{J_p}{J_0}$ is plotted in Fig. 7. As is apparent, in the vicinity of zero momentum it scales as

$$\frac{J_p}{J_0} \simeq 1 - \alpha |p|. \tag{C8}$$

As a consequence,

$$\frac{1}{L} \sum_p \langle \hat{b}_p^\dagger \hat{b}_p \rangle = \frac{1}{2\pi} \int_{-\pi}^{\pi} dp \left(\frac{1}{\sqrt{1 - (\gamma_p/\gamma_0)^2}} - 1 \right). \tag{C9}$$

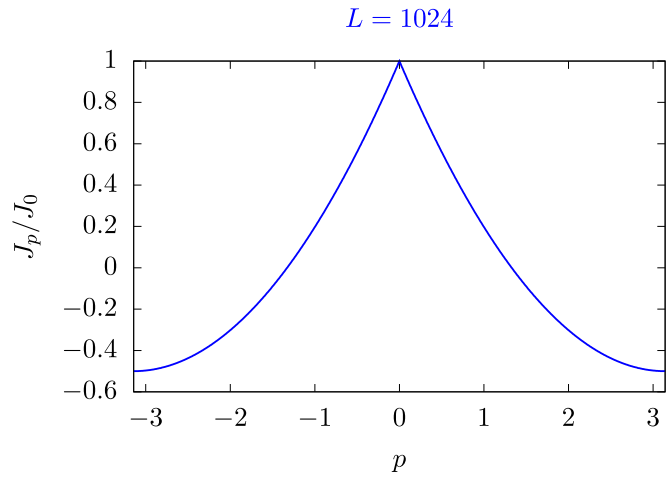

FIG. 7. J_p/J_0 for the SLAC hopping of Eq. (2).

In the vicinity of zero momentum, the integral takes the form, $\int_0^\Lambda dp \frac{1}{\sqrt{|p|}}$, and converges. Thereby fluctuations around the mean-field solution remain small and the spin-wave approximation is justified. Note that for short-ranged hopping, $\frac{J_p}{J_0} \simeq 1 - \alpha p^2$ such that $\frac{1}{L} \langle \hat{b}_p^\dagger \hat{b}_p \rangle$ diverges and fluctuations destroy the order.

Finally we compute the transverse spin-spin correlations:

$$\langle \hat{S}_r^z \hat{S}_0^z \rangle = \frac{S}{8\pi} \int_{-\pi}^{\pi} dp e^{ipr} \frac{1 - J_p/J_0}{\sqrt{1 - (J_p/J_0)^2}} \propto \frac{S}{8\pi} \int_{-\pi}^{\pi} dp e^{ipr} \sqrt{\alpha |p|} \propto \frac{1}{r^{1.5}}. \tag{C10}$$

This provides a very good match with the DMRG result.

[1] H. Nielsen and M. Ninomiya, Phys. Lett. B **105**, 219 (1981).
[2] D. B. Kaplan, Phys. Lett. B **288**, 342 (1992).
[3] M. Hohenadler, T. C. Lang, and F. F. Assaad, Phys. Rev. Lett. **106**, 100403 (2011).
[4] M. Hohenadler and F. F. Assaad, Phys. Rev. B **85**, 081106(R) (2012).
[5] S. D. Drell, M. Weinstein, and S. Yankielowicz, Phys. Rev. D **14**, 1627 (1976).
[6] T. C. Lang and A. M. Läuchli, Phys. Rev. Lett. **123**, 137602 (2019).
[7] Z.-X. Li, A. Vaezi, C. B. Mendl, and H. Yao, Sci. Adv. **4**, eaau1463 (2018).
[8] S. M. Tabatabaei, A.-R. Negari, J. Maciejko, and A. Vaezi, Phys. Rev. Lett. **128**, 225701 (2022).
[9] Y. Da Liao, X. Y. Xu, Z. Y. Meng, and Y. Qi, arXiv:2210.04272.
[10] B. H. Wellegehausen, D. Schmidt, and A. Wipf, Phys. Rev. D **96**, 094504 (2017).
[11] J. J. Lenz, B. H. Wellegehausen, and A. Wipf, Phys. Rev. D **100**, 054501 (2019).
[12] J. Lenz, L. Pannullo, M. Wagner, B. Wellegehausen, and A. Wipf, Phys. Rev. D **101**, 094512 (2020).
[13] C. L. Kane and E. J. Mele, Phys. Rev. Lett. **95**, 226801 (2005).
[14] F. D. M. Haldane, J. Phys. C **14**, 2585 (1981).
[15] T. Giamarchi, *Quantum Physics in One Dimension* (Clarendon Press, Oxford, 2004).
[16] Z.-X. Li, Y.-F. Jiang, and H. Yao, Phys. Rev. Lett. **117**, 267002 (2016).
[17] Z. C. Wei, C. Wu, Y. Li, S. Zhang, and T. Xiang, Phys. Rev. Lett. **116**, 250601 (2016).
[18] Z.-X. Li, Y.-F. Jiang, and H. Yao, Phys. Rev. B **91**, 241117(R) (2015).
[19] E. F. Huffman and S. Chandrasekharan, Phys. Rev. B **89**, 111101(R) (2014).
[20] F. F. Assaad, M. Bercx, F. Goth, A. Götz, J. S. Hofmann, E. Huffman, Z. Liu, F. P. Toldin, J. S. E. Portela, and J. Schwab, SciPost Phys. Codebases **1** (2022).
[21] R. Blankenbecler, D. J. Scalapino, and R. L. Sugar, Phys. Rev. D **24**, 2278 (1981).
[22] J. E. Hirsch, Phys. Rev. B **31**, 4403 (1985).
[23] S. White, D. Scalapino, R. Sugar, E. Loh, J. Gubernatis, and R. Scalettar, Phys. Rev. B **40**, 506 (1989).
[24] F. Assaad and H. Evertz, in *Computational Many-Particle Physics*, Lecture Notes in Physics, Vol. 739, edited by H. Fehske, R. Schneider, and A. Weiße (Springer, Berlin, 2008), pp. 277–356.
[25] P. Nason, Nucl. Phys. B **260**, 269 (1985).

[26] M. Weinstein, Phys. Rev. D **26**, 839 (1982).
[27] F. F. Assaad and D. Würtz, Phys. Rev. B **44**, 2681 (1991).
[28] M. Weber, D. J. Luitz, and F. F. Assaad, Phys. Rev. Lett. **129**, 056402 (2022).
[29] A. Messiah, *Quantum Mechanics* (Dover Publications, Mineola, NY, 1999).
[30] W. Kohn, Phys. Rev. **133**, A171 (1964).
[31] A. Auerbach, *Interacting Electrons and Quantum Magnetism*, Graduate Texts in Contemporary Physics (Springer, New York, 1994).
[32] M. F. Maghrebi, Z.-X. Gong, and A. V. Gorshkov, Phys. Rev. Lett. **119**, 023001 (2017).
[33] F. F. Assaad and I. F. Herbut, Phys. Rev. X **3**, 031010 (2013).
[34] See https://www.gauss-centre.eu.
[35] Jülich Supercomputing Centre, Journal of Large-Scale Research Facilities **5**, A171 (2019).
[36] M. Fishman, S. R. White, and E. M. Stoudenmire, SciPost Phys. Codebases **4** (2022).